BNL-101823-2014-TECH
AD/RHIC/RD/41;BNL-101823-2013-IR

Maximum Energy Deposition Densities in the Internal Dump

A. J. Stevens

June 1992

Collider Accelerator Department
Brookhaven National Laboratory

U.S. Department of Energy
USDOE Office of Science (SC)

Notice: This technical note has been authored by employees of Brookhaven Science Associates, LLC under Contract No.DE-AC02-76CH00016 with the U.S. Department of Energy. The publisher by accepting the technical note for publication acknowledges that the United States Government retains a non-exclusive, paid-up, irrevocable, world-wide license to publish or reproduce the published form of this technical note, or allow others to do so, for United States Government purposes.

DISCLAIMER

This report was prepared as an account of work sponsored by an agency of the United States Government. Neither the United States Government nor any agency thereof, nor any of their employees, nor any of their contractors, subcontractors, or their employees, makes any warranty, express or implied, or assumes any legal liability or responsibility for the accuracy, completeness, or any third party's use or the results of such use of any information, apparatus, product, or process disclosed, or represents that its use would not infringe privately owned rights. Reference herein to any specific commercial product, process, or service by trade name, trademark, manufacturer, or otherwise, does not necessarily constitute or imply its endorsement, recommendation, or favoring by the United States Government or any agency thereof or its contractors or subcontractors. The views and opinions of authors expressed herein do not necessarily state or reflect those of the United States Government or any agency thereof.

AD/RHIC/RD–41

RHIC PROJECT

Brookhaven National Laboratory

Maximum Energy Deposition Densities in the Internal Dump

A. J. Stevens

June 1992

Maximum Energy Deposition Densities in the Internal Dump

A.J. Stevens

I. Introduction

The most critical concern for the RHIC internal dump is survival of the dump "core" during extraction of the beam at full energy. This note describes energy deposition calculations and estimated response (temperature rise and stress) of dump core materials to this energy deposition for a specific set of assumptions describing the lattice parameters and the extraction kicker/sweeper.

II. Model for the Calculations

Energy deposition calculations were performed using a modified version of the hadron cascade Monte Carlo program CASIM.[1,2] The previous version of CASIM used to describe heavy ion interactions[2] assumed the Brandt-Peters formula for the nuclear interaction cross section and approximated the interaction process by multiplying final state probabilities of the physics model of the original CASIM[1] for nucleon, nucleus interactions by the atomic weight (A) of the incident projectile. The assumption is therefore that each nucleon in the projectile independently interacts with the target nucleus. While such an assumption is tenable for collisions where the projectile is smaller than the target ($A_p < A_t$) or for completely central collisions of equal mass nuclei, it makes very little sense when A_p exceeds A_t. In these cases, a simple geometric picture of the collision process suggests that a part of the projectile is "sheared off" and indeed heavy fragments from peripheral heavy ion collisions have been observed and studied at both LBL and CERN.[3,4] The following changes were made to CASIM to incorporate fragments.

(1) The Brandt-Peters formula for the interaction cross section was replaced by the geometric cross section:

$$\sigma = \pi(1.25(A_p^{1/3} + A_t^{1/3})^2 \text{ X } 10^{-26} \text{ cm}^2$$

which corresponds to two nuclei with radii $r_i = 1.25A_i^{1/3}f$ interacting with impact parameter b between 0 and b_{max} where $b_{max} = \max(r_p, r_t)$.

(2) When an interaction occurs during heavy ion transport, a random impact parameter is chosen and the intersection of a cylinder with radius r_t displaced by this impact parameter with a sphere of radius r_p is calculated. The ratio of this volume of intersection to the volume of the projectile sphere is interpreted as the fraction of nucleons in the projectile which interact with the target nucleus. If this fraction (f) is less than 1, a random number selection determines whether to perform the interaction (again, with the original physics

model of CASIM) or to transport a fragment whose Z and A values are decreased from those of the incident projectile by (1-f).

(3) If a fragment is created it is given a P_t "kick" selected from a Gaussian distribution whose 1 σ value is 41.4•Sqrt(4•F•(B-F)/(B-1)) MeV/c where B is the A value of the incident ion and F is the A value of the fragment. This expression follows from the fitted function of Ref. 3 assuming constant (A independent) Fermi momentum and corresponds to a P_t per nucleon change of the order of 10 Mev/c which has been observed to be independent of incident momentum for ^{16}O beams.[4] This small energy exchange between the interaction products and fragments justifies the approach here which treats the fragments as "spectators."

III. Geometry/Lattice Functions

The dump core geometry is based on the preliminary conceptual design[5] and preliminary calculations of the effects of energy which escapes the internal dump on downstream magnets.[6] The beam enters the dump through a thin titanium window which is immediately followed by a region of graphite. A transition from graphite to steel occurs at some values of the transverse (R) and beam direction (Z) coordinates. A "beams eye view" of the geometry assumed for the calculations reported here is shown in Fig. 1. The beam as shown is assumed to have been kicked a vertical distance ΔY and to occupy an area $\delta X \delta Y$ where δY is determined from the beam size and the δX spread is achieved by a beam sweeper.[7] In the remainder of this note δX = 2 cm. is assumed so that the beam area, containing 68% of the beam, is given by $4\sigma_V$ cm^2 where σ_V is the 1-sigma value of the vertical beam size.[8] Although the transition from graphite to steel is taken here to occur at R=7 cm. and Z=150 cm., these values are not meant to be definitive. As the transition boundary in Z moves closer to the dump entrance, the energy deposition in the steel becomes greater but energy which escapes the dump aperture becomes less, so the actual choice of the boundary is a compromise between these two effects. Factors which determine the R transition boundary are discussed in section V below.

The beam characteristics when extraction occurs vary with the tune of the insertion regions which has a wide range of values. Shown in Table I below are approximate lattice functions[9] at a position 31 m. downstream of Q3 (outer arc), which is taken to be the position of the entrance face of the dump. The beam areas in this table (A_b) are for a swept Au beam as described above, i.e.- $4\sigma_V$ cm^2, for invariant emittance values of 10π and 60π mm-mrd. It will be assumed that the 10π emittance value pertains at all energies for all ion species except Au. For Au, the assumption is that 10π is appropriate for injection at 10.4 GeV/u but that at the full energy of 100 GeV/u, allowance must be made for running at both 10π and 60π values of the invariant emittance.

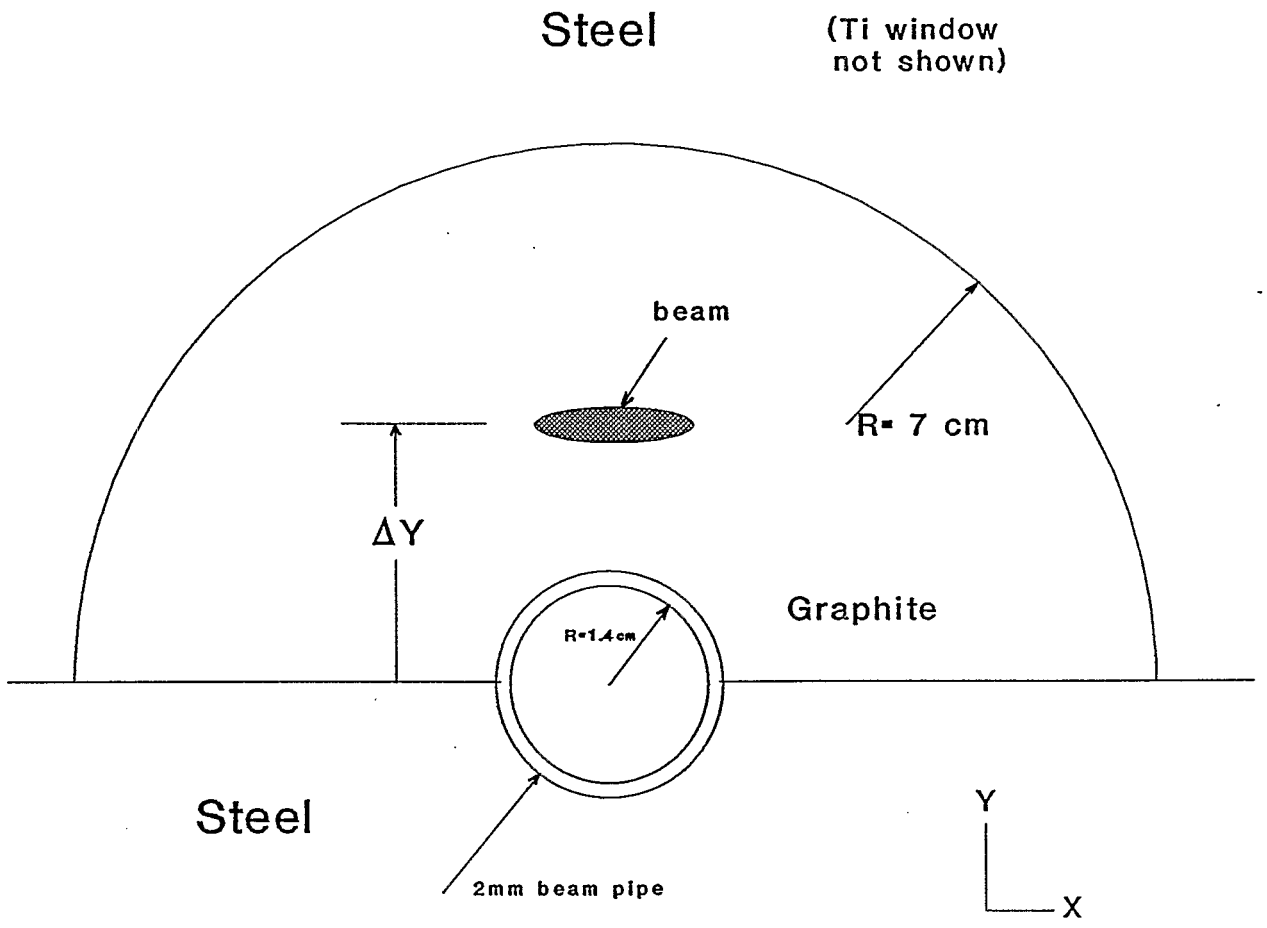

Fig. 1 Schematic View of the Dump Face

Table I. Approximate Lattice Functions at the Dump Entrance for Various Crossing Point β^* Values

β^* (m)	β_V (m)	α_V	β_H (m)	α_H	$A_b(10\pi)$ (cm^2)	$A_b(60\pi)$ (cm^2)
10	25.2	.889	21.2	-1.062	.249	.610
6	39.8	1.625	13.2	-0.820	.313	.767
2	89.0	4.914	3.91	-0.246	.468	1.146
1	152.2	9.580	2.05	0.169	.612	1.489
0.5	246.1	17.96	2.67	1.227	.778	1.906

The largest beam size (for Au beams at $\beta^*=0.5$ m. and 60π emittance), when combined with a limit on energy which escapes the dump through the beam aperture, sets the minimum value of ΔY in Fig. 1 and thus defines the required vertical displacement on the dump face that the kicker must achieve. In this note it will be assumed that the vertical beam tail, defined as the 2.5σ value, must be at least 1.7 cm. from the edge of the dump aperture. This value is believed to provide a sufficient margin of safety against quenching Q4O, the magnet immediately downstream of the dump.[6] The value of ΔY then becomes $1.4 + 1.7 + 2.5\sigma_V = 4.3$ cm. for the largest beam.

IV. Materials Properties

As discussed above, the generic materials of concern here are titanium, steel, and graphite. For titanium and steel, we retain the specific materials described in Ref. 5. For graphite, we adopt a set of "typical" values for ATJ graphite.[10] Table II shows the assumed properties.

Table II. Assumed Material Properties at Room Temperature

Material		Density (g/cc)	Specific Heat (cal/g°C)	Coefficient of Thermal Expansion ($X10^{-6}$/°C)	Melting Point (°C)	Tensile Strength (Kpsi)	Compressive Strength (Kpsi)	Elastic Modulus (Mpsi)
Titanium (Ti-6Al-4V)		4.5	0.135	9.54	1649	170.	-	16.5
Steel (AISI 430)		7.8	0.110	10.44	1482	90.	-	29.0
Graphite (ATJ)	wg	1.8	0.170	2.2	≈3500	3.92	8.28	1.41
	ag			5.0		3.63	8.15	1.38

In Table II, the symbols "wg" and "ag" for graphite refer to "with" and "against" the grain direction. Ductile materials such as steel and titanium can withstand enormous

stresses in compression and, in general, limits for ductile materials in compression are not measurable.[11] Graphite, in contrast, has definite limits for both tensile and compressive stresses, although the compressive strength is much higher as indicated. Thermal stresses which arise from rapid heating during a beam dump have both tensile and compressive components and these will be carefully distinguished when evaluating the response of the dump materials in section VI below.

V. Energy Deposition Calculations

Energy deposition in the thin (<1 mm.) titanium window is straightforwardly obtained from dE/dX. The worst case considered here is for the $\epsilon = 10\pi$, $\beta^* = 10$m Au beam. In this case one obtains, for the design intensity of 57 X 10^9 ions,

$$\begin{aligned} E_d &= 57 \text{ X } 10^9 \text{ X } (79)^2 \text{ X } 1.6 \text{ X } 10^{-3} \text{ GeV}/(\text{g/cm}^2) \text{ X } (.68/.249 \text{ cm}^2) \\ &= 1.55 \text{ X } 10^{12} \text{ GeV/g} \\ &= 59.2 \text{ cal/g} \end{aligned}$$

To obtain energy deposition densities in the interior regions, CASIM calculations, with the heavy ion code modified as described in section II above, were performed for Au at 100 GeV/u and for protons at both 100 GeV/c and 250 Gev/c. The initial transverse displacement of primaries was assumed to be uniform in the X coordinate (± 1 cm.) and Gaussian in Y, and the initial divergences were obtained from the lattice functions at the dump face (Table I) to which the Y angular kick, $\Delta Y/2500$ cm., was added.

The maximum energy deposition density is always within a volume whose transverse coordinates are within the core of the beam. For this reason energy deposition was calculated in beam-centered bins whose transverse X width was ± 0.5 cm. and whose Y width was $\pm 1\sigma_V$. In addition, energy deposition was binned within a restricted azimuth ($|\tan\phi| < 0.5/\Delta Y$ with respect to the Y axis) in the beam pipe and over a more extensive grid with $\Delta R = 0.54$ cm. within the same restricted azimuth. The latter grid served for evaluation of the maximum energy deposition in steel at both the longitudinal ($Z > 150$ cm.) and radial ($R > 7$ cm.) transitions.

Fig. 2 shows the energy deposition density vs. Z in the beam core for the smallest and largest Au beams considered here. As illustrated by the results of Fig. 2, the maximum energy density scales approximately as the inverse of the beam size. The maximum energy density in the graphite always occurs at (for Au) or near (for protons) the beginning of the dump and the maximum energy density in steel follows the $Z = 150$ cm. transition. Table III below shows these maximum energy densities as a function of primary type for the design beam intensity, i.e., either 5.7 X 10^{10} Au ions or 5.7 X 10^{12} protons. The statistical error on the energy densities in Table III, determined from multiple computer runs with different random number seeds, is $\leq 6\%$.

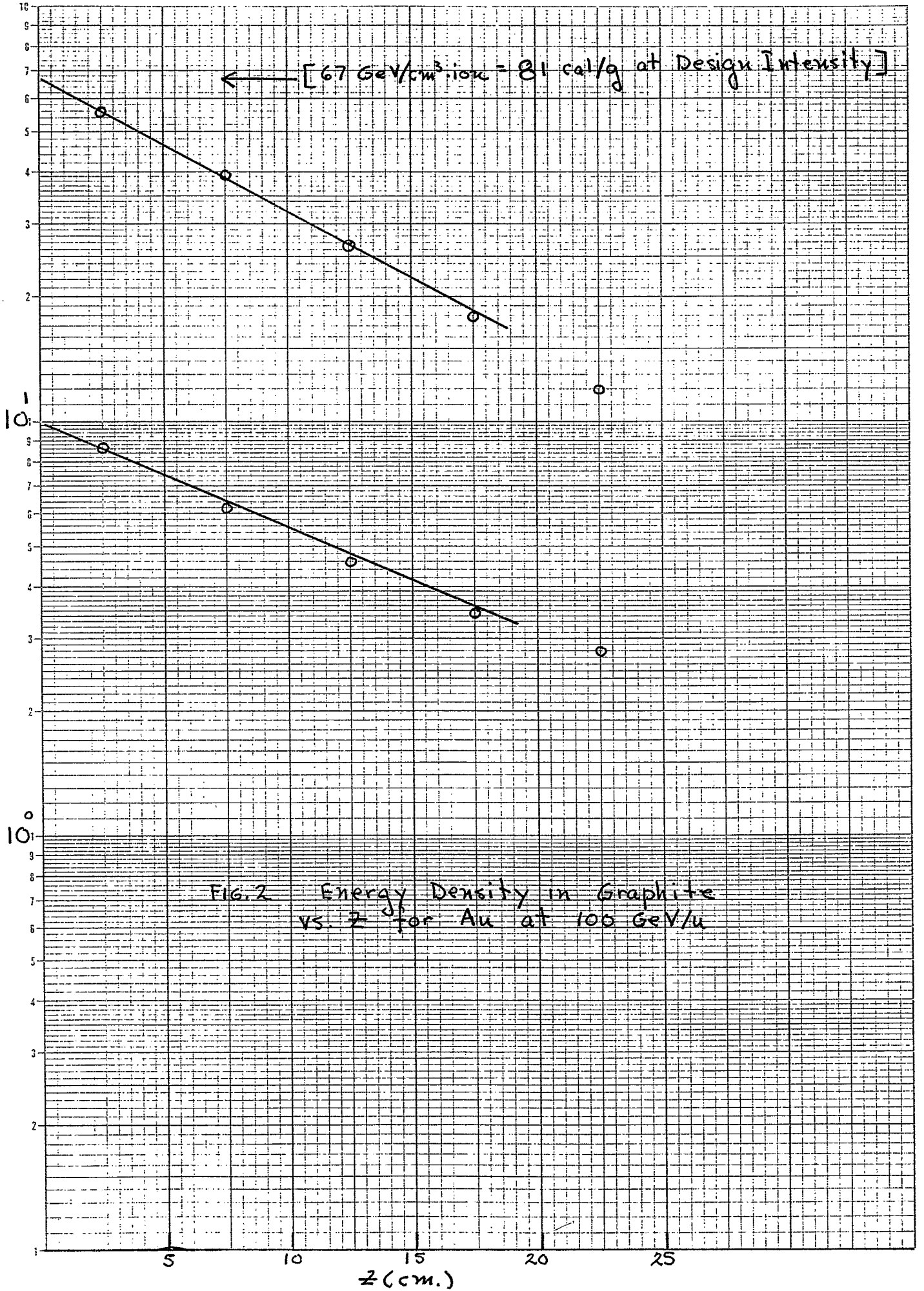

FIG. 2 Energy Density in Graphite vs. Z for Au at 100 GeV/u

SEMI-LOGARITHMIC 3 CYCLES X 70 DIVISIONS AD-0837-60

Table III. Maximum Energy Density by Location and Primary Type for Design Intensity

Beam Type	Beam Area (cm^2)	E_{max} graphite (cal/g)	E_{max} steel (Z>150 cm.) (cal/g)
Au @ 100 GeV/u	0.249	81.0	2.15
protons @ 100 GeV/c	0.249	1.94	1.92
protons @ 250 GeV/c	0.158	3.40	12.2

As will be shown in the next section, the high (81.0 cal/g) energy in graphite at the dump entrance for the smallest Au beam is the most severe condition. For comparison with this value, computer runs were made for the smallest ($\epsilon = 10\pi$, $\beta^* = 10$m) iodine beam at 104 GeV/u. At the design intensity (8.55×10^{10} ions), the corresponding energy density in graphite is 58 cal/g.

As mentioned above, calculations were also made to obtain the energy densities in the transverse steel boundaries, i.e., in the beam pipe and R>7cm. regions for Z<150 cm. These regions are manifestly sensitive to the ΔY kick displacement, so that comparison runs were made between the nominal ΔY = 4.3 cm. displacement and ΔY values which are "too close" to the boundaries in question. These were (arbitrarily) taken to be ΔY = 3.6 cm. for the beam pipe and ΔY = 5.3 cm. for the R>7cm. region. In these calculations, the largest beams ($\beta^* = 0.5$m, $\epsilon = 10\pi$ for protons and 60π for Au) result in the highest energy densities because the vertical beam "tail" is closer to the transverse boundary. The results are shown in Table IV below.

Table IV. Highest Energy Densities at Design Intensity in Steel Regions Transverse to the Beam

Beam Type	Beam Area (cm^2)	E_{max} beam pipe (cal/g)	E_{max} R>7cm. (cal/g)
Au @ 100 GeV/u	1.906	~0.70 @ ΔY=3.6 ~0.49 @ ΔY=4.3	0.92 @ ΔY=5.3 0.50 @ ΔY=4.3
protons @ 100 GeV/c	.495	~0.25 @ ΔY=3.6 ~0.17 @ ΔY=4.3	~0.40 @ ΔY=5.3 ~0.21 @ ΔY=4.3
protons @ 250 GeV/c	.778	~0.56 @ ΔY=3.6 ~0.39 @ ΔY=4.3	0.99 @ ΔY=5.3 ~0.49 @ ΔY=4.3

The "~" sign on the entries in Table IV indicate a relatively high (10-50%) estimated statistical error.

All the entries in Table IV are small in comparison with the 12.2 cal/g in steel in Table III which will be shown to be tolerable in the next section. Since the $\Delta Y = 5.3$cm. displacement compensates for ignoring the actual lateral asymmetry in the sweep[7], the R = 7 cm. boundary would seem to be sufficient. However, another sweeping scheme is being studied[14] wherein the sweep is in the same direction as the kick. If this were adopted, the graphite region would need to extend to a greater distance in this direction. Another reason for extending the lateral graphite region would be to allow for a stronger kicker and/or sweeper.

VI. Materials Response

The energy deposited in the dump core produces a sharp temperature rise and concomitant thermal stress. To estimate the stresses involved, we follow the procedure of Sievers[12] who has calculated both static and dynamic stresses in the context of a model wherein a longitudinally and radially constrained cylinder (or radially constrained disk) of radius R_o is subjected to a rapid rise to the constant temperature ΔT in a region $r \leq r_o$ where $r_o < R_o$. Sievers has shown that dynamic enhancements over the static stresses are small, even in the symmetric model which exaggerates such enhancements, when the temperature increase has a finite rise time (~ 12.6 μsec for RHIC). In this model, assuming $r_o << R_o$, the maximum static stresses are the following:

Disk:

$$\sigma_{max}(\text{tension}) = (Y \cdot \alpha \cdot \Delta T)/2 \quad \text{(azimuthally)}$$

$$\sigma_{max}(\text{compression}) = (Y \cdot \alpha \cdot \Delta T)/2 \quad \text{(radially and azimuthally)}$$

Cylinder:

$$\sigma_{max}(\text{tension}) = (Y \cdot \alpha \cdot \Delta T)/2(1-\nu) \quad \text{(azimuthally)}$$

$$\sigma_{max}(\text{compression}) = (Y \cdot \alpha \cdot \Delta T)/2(1-\nu) \quad \text{(radially and azimuthally)}$$

$$= (Y \cdot \alpha \cdot \Delta T)/(1-\nu) \quad \text{(longitudinally)}$$

where Y is the elastic modulus, α is the coefficient of thermal expansion, and ν is the Poisson ratio which is assumed here to be 1/3. In these formula, the compressive stresses are within the heated region ($r < r_o$) and the tensile stress is in the initially "cool" region outside r_o, and results from the hot region expanding radially which exerts an azimuthal "pull" on the immediately adjacent cool material. In fact, the azimuthal stress is discontinuous at r_o, which results from the step function in temperature at r_o in this simple model. As mentioned above, for the ductile titanium window and steel regions, the thermal tension stress must be compared with the tensile strength (TS) whereas for graphite, both tension and compressive stresses must be compared with the corresponding strengths.

From the above equations, the materials properties in Table II, and the **worst case** energy deposition densities calculated in section V, the maximum thermal stresses for the RHIC design intensity can be estimated. The results are given in Table V below.

Table V. Maximum Temperature Rises and Thermal Stresses for Design Intensity

Material	ΔT(max) (°C)	σ_{max}/TS	σ_{max}/CS	Beam (for $\epsilon = 10\pi, \beta^* = 10$m)
Ti window	438.5	0.20	-	Au @ 100 GeV/u
Steel	110.9	0.28	-	protons @250 GeV/c
Graphite	476.5	0.68	0.30	Au @ 100 GeV/u

In this table, the disk stress formula apply for the titanium window and the cylinder formula for graphite and steel. The graphite has been taken with the grain in the longitudinal direction which gives the maximum compressive stress to strength ratio of 0.30, as shown in the table, in the radial or azimuthal directions. This ratio is slightly less (0.27) in the longitudinal direction.

VII. Discussion of Results

At the RHIC beam design intensities, 5.7 X 10^{10} 100 GeV/u Au ions or 5.7 X 10^{12} 250 GeV/c protons, the estimated worst case temperature rises and accompanying thermal stresses for the titanium window (438 °C and 20% of tensile strength) and steel portion of the dump core (111 °C and 28% of tensile strength) are well within tolerable limits. CERN experience has shown that Ti windows can operate indefinitely at the same energy deposition density as calculated for the worst case RHIC conditions,[13] and stress limits for steel (determined by fatigue) are typically set at one-half the tensile strength.[11]

The estimated worst case azimuthal tensile stress in the graphite, 68% of tensile strength, is of more concern, but is ameliorated by the simplicity of the model assumed; in fact the radial temperature gradient which the model ignores will act to relieve the actual tensile stress. Given this fact and the uncertainty in graphite properties mentioned in section IV, the best estimate of the actual worst case stress is **approximately** one-half the strength. It should be clear, however, that the graphite section of the internal dump core evaluated here is at the limit of prudent design practice and that any significant increase in the Au beam intensity will likely require major changes in the beam extraction systems.

References/Footnotes

1. A. Van Ginneken, "CASIM. Program to Simulate Hadronic Cascades in Bulk Matter," Fermilab FN-272, 1975.

2. A. Stevens, "Improvements in CASIM; Comparison with Data," AGS/AD/Tech. Note No. 296, 1988.

3. D.E. Greiner, et. al., "Momentum Distributions of Isotopes Produced by Fragmentation of Relativistic ^{12}C and ^{16}O Projectiles," Phys. Rev. Lett. **35**, p.152, 1975.

4. G. Gerbier et. al., "Charges and Angular Distributions of Fast Fragments Produced in 3.2-TeV ^{16}O Collisions with Pb," Phys. Rev. Lett. **59**, p.2535, 1987.

5. A.J. Stevens, "RHIC Internal Beam Dump: Preliminary Conceptual Design," RHIC Tech. Note. No. 43, 1988.

6. A.J. Stevens, "Preliminary Study of Energy Deposition Downstream of the Internal Dump," AD/RHIC/RD-33, 1992.

7. Although Fig. 1 shows symmetry in the X (sweep) direction, the actual sweep obtains an X spread which begins at X=0. Symmetry is assumed here for calculational convenience.

8. The 1-sigma value is defined by $\sigma^2 = \beta \cdot \epsilon/(6\pi \cdot \beta\gamma)$ where ϵ is the invariant emittance and $\beta\gamma = P/M$.

9. At the time of this writing, the lattice parameters are not finalized. The Q3O lattice parameters assumed here were provided by H. Foelsche.

10. R. Werbeck, LANL, private communication. The values relate to a specific grade of graphite blocks produced by Union Carbide. It should be noted that graphite properties vary widely, so that the properties listed in Table II are by no means definitive.

11. S. Timoshenko, "Strength of Materials, Part II,", Robert E. Krieger, Huntington, NY, 1958.

12. P. Sievers, "Elastic Stress Waves in Matter Due to Rapid Heating by an Intense High-Energy Particle Beam,", CERN LAB II/BT/74-2, 1974.

13. P. Sievers, private communication. Titanium windows operate successfully at CERN at intensities of 10^{13} protons/mm^2. This is (fortuitously) the same energy deposition density as calculated in section V of the text.

14. H. Foelsche, private communication.